4,4′,5,5′-Tetracarboxy-2,2′-bipyridine Ru(II) Sensitizers for Dye-Sensitized Solar Cells

ARTICLE *in* INORGANIC CHEMISTRY · JULY 2014

Impact Factor: 4.76 · DOI: 10.1021/ic501178f · Source: PubMed

8 AUTHORS, INCLUDING:

Kuan-Lin Wu
National Tsing Hua University
21 PUBLICATIONS **631** CITATIONS
SEE PROFILE

Tainan Duan
King Abdullah University of Science and Techn…
11 PUBLICATIONS **96** CITATIONS
SEE PROFILE

Yun Chi
National Tsing Hua University
346 PUBLICATIONS **10,858** CITATIONS
SEE PROFILE

Inorganic Chemistry

Article

pubs.acs.org/IC

4,4′,5,5′-Tetracarboxy-2,2′-bipyridine Ru(II) Sensitizers for Dye-Sensitized Solar Cells

Chun-Cheng Chou,[†] Fa-Chun Hu,[†] Kuan-Lin Wu,[†] Tainan Duan,[†] Yun Chi,*[,†] Shih-Hung Liu,[‡] Gene-Hsiang Lee,[‡] and Pi-Tai Chou*[,‡]

[†]Department of Chemistry and Low Carbon Energy Research Center, National Tsing Hua University, Hsinchu 30013, Taiwan

[‡]Department of Chemistry and Center for Emerging Material and Advanced Devices, National Taiwan University, Taipei 10617, Taiwan

Supporting Information

ABSTRACT: Two Ru(II) sensitizers TCR-1 and TCR-2 bearing four carboxy anchoring groups were prepared using 4,4′,5,5′-tetraethoxycarbonyl-2,2′-bipyridine chelate and 4-(5-hexylthien-2-yl)-2-(3-trifluoromethyl-1*H*-pyrazol-5-yl)pyridine and 6-*t*-butyl-1-(3-trifluoromethyl-1*H*-pyrazol-5-yl)-isoquinoline, respectively. Dissolution of these sensitizers in DMF solution afforded a light green solution up to 10^{-5} M, for which their color gradually turned red upon further dilution and deposition on the surface of a TiO_2 photoanode due to the spontaneous deprotonation of carboxylic acid groups. These sensitizers were characterized using electrochemical means and structural analysis time-dependent density functional theory (TDDFT) simulation and were also subjected to actual device fabrication. The as-fabricated DSC devices showed overall efficiencies η = 6.16% and 6.23% versus their 4,4′-dicarboxy counterparts TFRS-2 and TFRS-52 with higher efficiencies of 7.57% and 8.09%, using electrolyte with 0.2 M LiI additive. Their inferior efficiencies are possibly caused by the combination of blue-shifted absorption on TiO_2, inadequate dye loading, and the perpendicularly oriented central carboxy groups.

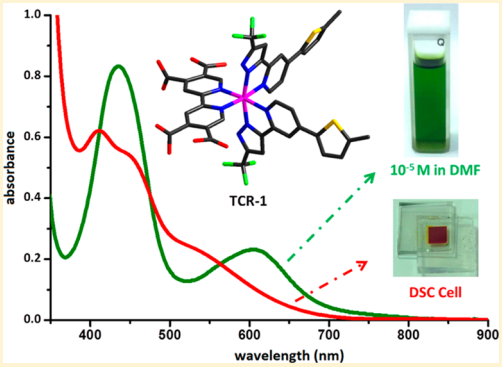

INTRODUCTION

Dye-sensitized solar cells (DSCs) are considered to be a leading contender to the emerging photovoltaics,[1] complementary to other modern competing technologies such as organic photovoltaics[2] and Pervoskite cells.[3] These DSC devices were typically fabricated by depositing a sensitizer on a mesoporous TiO_2 electrode, together with incorporation of an electrolytic solution with an I^-/I_3^- redox couple for rapid dye regeneration, and a Pt-based counter electrode for reducing the oxidized I_3^- ions. Despite rapid progression, DSC dye design remains one of the most challenging areas and has been attracting extensive research activities into the Ru(II) metal,[4] organic push−pull dyes,[5] squaraine dyes for transparent solar cells,[6] and zinc porphyrin relevant sensitizers,[7] among which superior DSC efficiencies have been reported. In most cases, they were strategically designed by incorporation of bulky substituents at the basal skeleton of dyes to suppress intermolecular aggregation,[8] or by addition of one or more carboxy groups that can tightly bind the TiO_2 photoanode for increasing device stability. Notably, the Ru(II) sensitizers with a single carboxy group always showed inferior efficiency,[9] whereas those with multiple carboxy groups, such as 4,4′-dicarboxy-2,2′-bipyridine, 4,4′,4″-tricarboxy-2,2′:6′,2″-terpyridine, and analogues,[10] have exhibited the highest conversion efficiency reported among sensitizers with optimal device stability. As for the 2,2′-bipyridine chelate, the effect on reshuffling the substituents or carboxy anchor from 4,4′- to either 3,3′- or 5,5′-positions was evaluated, and their performances were then compared with that of the benchmark Ru sensitizer, N719,[11] or their respective parent metal complexes.[12] With an aim to further investigate the functional behaviors of these 2,2′-bipyridine anchors, we proceed to design and synthesize the Ru(II)-based complexes with unprecedented four carboxylic acid groups on the single 2,2′-bipyridine anchor, e.g., the 4,4′,5,5′-tetracarboxy-2,2′-bipyridine, with the hope to probe the photophysical properties and cell characteristics, for which the extra carboxy groups may hopefully induce stronger binding to TiO_2, increase the absorption extinction coefficient, and cause the red-shifting of absorption profile for better response to solar irradiation.

RESULTS AND DISCUSSION

As shown in Scheme 1, the 4,4′,5,5′-tetraethoxycarbonyl-2,2′-bipyridine anchor was prepared using a multistep protocol starting from ethyl cinchomeronate, followed by *m*-chloroperoxybenzoic acid (mCPBA) oxidation and chlorination with $POCl_3$, chloride-to-bromide metathesis using bromotrimethylsilane, and coupling of the resulting 6-bromo-3,4-diethoxycarbonylpyridine in the presence of $Sn_2Bu^n_6$ and $PdCl_2(PPh_3)_2$ by employing Stille coupling.[13]

Received: May 21, 2014
Published: July 29, 2014

   dx.doi.org/10.1021/ic501178f | *Inorg. Chem.* 2014, 53, 8593−8599

Scheme 1[a]

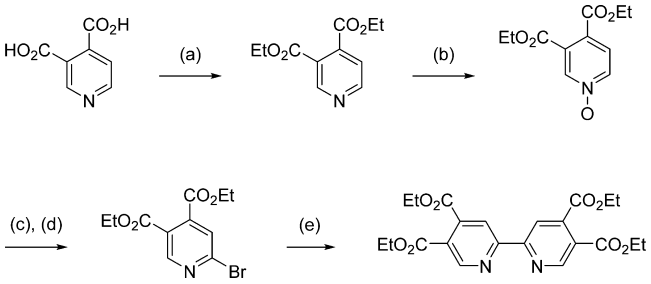

[a]Synthetic protocols: (a) H_2SO_4, EtOH, reflux; (b) mCPBA, CH_2Cl_2, rt; (c) $POCl_3$, reflux; (d) $SiBrMe_3$, propionitrile, reflux; (e) $Sn_2Bu^n_6$, $PdCl_2(PPh_3)_2$, toluene, reflux.

This anchoring chelate was then reacted with $[RuCl_2(p\text{-cymene})]_2$ in dimethylformamide (DMF) and with each of two tailor-made ancillaries, namely, 4-(5-hexylthien-2-yl)-2-(3-trifluoromethyl-1*H*-pyrazol-5-yl)pyridine and 6-*t*-butyl-1-(3-trifluoromethyl-1*H*-pyrazol-5-yl)isoquinoline, in refluxing xylenes. Flash column chromatography and subsequent hydrolysis in basic media yield the demanded tetracarboxy Ru(II) complexes, coded TCR-1 and TCR-2, in ∼30% yields (Scheme 2).

Scheme 2. Structural Drawings of the Studied Ru(II) Sensitizers

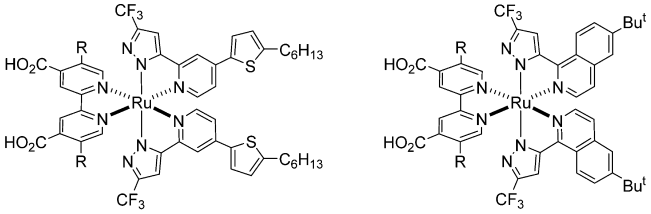

R = CO_2H, TCR-1
R = H, TFRS-2
R = CO_2H, TCR-2
R = H, TFRS-52

For confirming their structural features, single-crystal X-ray analysis of ester substituted derivative TCR-1-Et was carried out, for which the perspective view and the associated metric parameters are shown in Figure 1. As can be seen, the molecule consists of a distorted octahedral framework with Ru−N distances spanning the narrow range of 2.023(1)−2.084(9) Å. All chelates seem to be planar, and the azolate fragments adopt the expected *trans*-orientations. The thienyl appendages on the azolate chelate also exhibit small dihedral angles of 20.2° and 22.8°, showing excellent π-conjugation extended over these ancillaries. As for the bipyridine anchor, the outer ethoxycarbonyl groups at both the 5- and 5′-positions adopt the essentially parallel orientation with dihedral angles of 10−22° relative to the basal plane of bipyridine. In sharp contrast, the central ethoxycarbonyl groups at the 4- and 4′-sites are rotated by 77−81°, for which this perpendicular orientation indicates a severe disruption of π-conjugation.

We are then very curious about whether the carboxy groups for the hydrolyzed TCR-1 and TCR-2 are similar to ethoxycarboxy groups of TCR-1-Et at the 4- and 4′-sites, being subject to significant deviation from the planarity versus bipyridine. To gain insight into this issue, we then executed the ground-state geometry optimization of the studied sensitizers obtained from the density functional theory (DFT) method. As

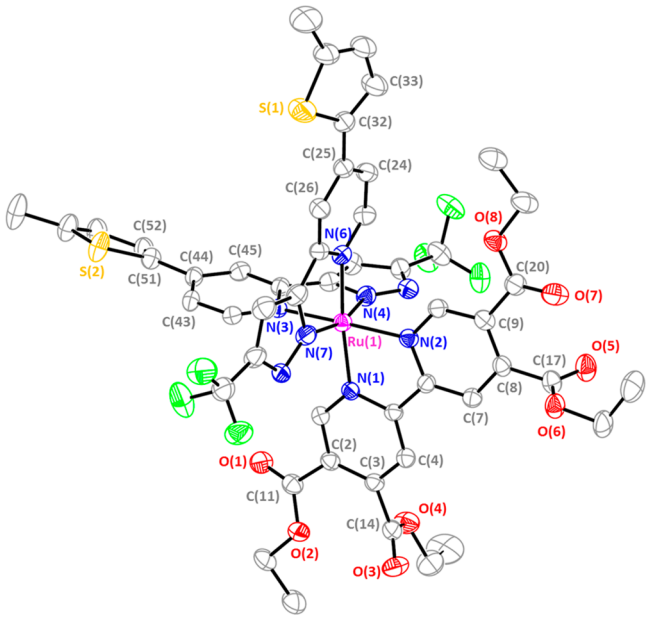

Figure 1. Perspective view of TCR-1-Et. Only one carbon for hexyl groups is shown, the hydrogen atoms were omitted for clarity, and the thermal ellipsoids were drawn at the 30% probability level. Selected bond lengths: Ru1−N1 = 2.023(1) Å, Ru1−N2 = 2.030(7) Å, Ru1−N3 = 2.084(9) Å, Ru1−N4 = 2.043(2) Å, Ru1−N6 = 2.066(3) Å, and Ru1−N7 = 2.030(6) Å. Selected bond angles: N1−Ru1−N6 = 171.8(7)°, N2−Ru1−N3 = 173.4(5)°, N4−Ru1−N7 = 165.3(2)°. Selected dihedral angles: plane (C2, C3, C4)−plane (C11, O1, O2) = 21.8°, plane (C2, C3, C4)−plane (C14, O3, O4) = 76.7°, plane (C7, C8, C9)−plane (C20, O7, O8) = 9.8°, plane (C7, C8, C9)−plane (C17, O5, O6) = 81.1°, plane (C24, C25, C26)−plane (S1, C32, C33) = 22.8°, plane (C43, C44, C45)−plane (S2, C51, C52) = 20.2°.

a result, the simulated 4,4′-dicarboxy-2,2′-bipyridine dihedral angles are (21.11°, 25.66°) for TCR-1 and (25.39°, 26.76°) for TCR-2, which are notably deviated from 0°. In comparison, the 4,4′-dicarboxy-2,2′-bipyridine dihedral angles of their analogues bearing 4,4′-dicarboxy-2,2′-bipyridine chelate, i.e., TFRS-2 and TERS-52, are calculated to be (0.79°, 0.30°) and (0.43°, 0.33°) for TFRS-2 and TFRS-52, respectively, giving a nearly planar configuration. For short, these calculated molecular structures seem to suggest the existence of reduced steric congestion between the carboxylic acid groups versus the ethoxycarbonyl groups of the ester counterparts. In fact, a recent study of Ru(II) sensitizer bearing an *ortho*-dicarboxyphenylterpyridine anchoring unit also showed similar distortion of the carboxylic acid groups by computer simulation.[14]

To examine whether the above-mentioned molecular geometry is also applicable to the dye adsorption onto the TiO_2 nanocrystals, we then further simulated the interacting mode with the anatase (101) $(TiO_2)_{38}$ surface.[15] The calculated 4,4′-dicarboxy-2,2′-bipyridine dihedral angles of TFRS-2/$(TiO_2)_{38}$, TFRS-52/$(TiO_2)_{38}$, TCR-1/$(TiO_2)_{38}$, and TCR-2/$(TiO_2)_{38}$ are recorded to be (0.16° and 0.31°), (0.85° and 3.97°), (25.66° and 25.04°), and (28.47° and 29.75°), respectively. As a result, when TFRS-2 and TFRS-52 are anchored onto the TiO_2 surface, it is reasonable to expect that their 4,4′-dicarboxy-2,2′-bipyridine dihedral angles are nearly unchanged, similar to those of the free dye molecule. For TFRS-2/$(TiO_2)_{38}$ and TFRS-52/$(TiO_2)_{38}$, the approaching coplanar dihedral 4,4′-dicarboxy-2,2′-bipyridine makes a perfect π-conjugation pathway that facilitates the interfacial charge

dx.doi.org/10.1021/ic501178f | Inorg. Chem. 2014, 53, 8593−8599

injection. Conversely, due to the perpendicularly arranged 4,4′-dicarboxy-2,2′-bipyridine fragments and hence a disrupted π-conjugation, the charge injection may be hampered in the cases of TCR-1/$(TiO_2)_{38}$ and TCR-2/$(TiO_2)_{38}$ (vide infra).

The absorption spectra of TCR-1 and TCR-2 in DMF are measured and are shown in Figure 2. In addition to the higher

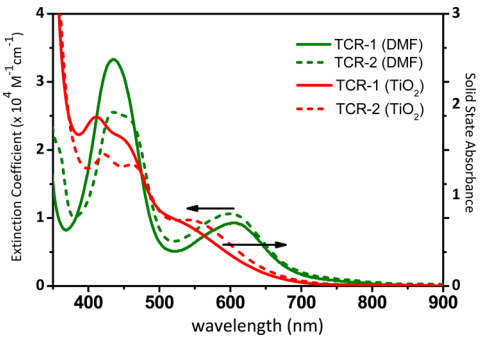

Figure 2. UV−vis absorption spectra of TCR-1 and TCR-2 in DMF (solid line, left axis) and those deposited on TiO_2 thin film (dashed line, right axis).

energy $\pi\pi^*$ transition at ∼436 nm, both complexes exhibit strong absorption with a peak wavelength at ∼604 nm. The valley of the absorption spectrum at ∼510 nm gave them a distinctive green color in solution (10^{-4} M). On the basis of the time-dependent DFT (TDDFT) simulations in DMF (see the Supporting Information for details), the simulated absorption peaks of TCR-1 (TCR-2) at 759.7 (756.8), 606.8 (619.7), 458.4 (460.1), and 416.7 (413.6) nm (see Figure 3 for TCR-1

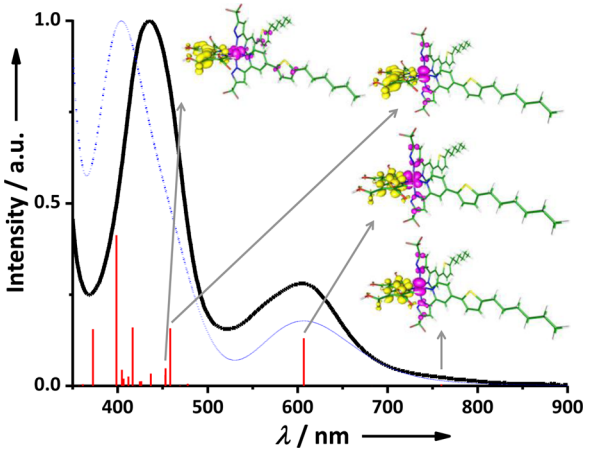

Figure 3. Experimental (black solid line) and TDDFT calculated (blue dashed line) absorption spectra of TCR-1 in DMF (a Gaussian convolution σ = 0.2 eV for spectral fitting). For clarity, the calculated absorption wavelengths (red vertical lines) and the relative transition probabilities (magnitude of vertical lines) are shown. Also displayed are frontier orbitals (pink color: occupied orbital; yellow color: unoccupied orbital) that relate to the major transitions.

and Figure S1, Supporting Information, for TCR-2) are attributed to the metal-to-ligand charge-transfer (MLCT) excitation. The lowest singlet optical transition ($S_0 \rightarrow S_1$) of TCR-1 and TCR-2 located at 759.7 and 756.8 nm, respectively, is assigned to the HOMO → LUMO transition (see Tables S1 and S2, Supporting Information), which is ascribed to the metal-to-bipyridine MLCT transition, together with a small amount of ligand-to-ligand charge transfer (LLCT) involving pyrazolate ancillaries. Furthermore, the electron distributions of LUMO, LUMO+1, and LUMO+2 molecular orbitals of TCR-1 and TCR-2 are localized at the 4,4′,5,5′-tetracarboxy-2,2′-bipyridine anchor (see Figures S2 and S3, Supporting Information), which are beneficial to the excited-state electron injection. Note that the peaks at 452.9 nm for TCR-1 and 503.6 nm for TCR-2 are accompanied by a minor part of LLCT from the thienyl (TCR-1) or quinolinyl fragment (TCR-2) to the 4,4′,5,5′-tetracarboxy-2,2′-bipyridine anchor.

Upon depositing these samples onto TiO_2, the higher energy $\pi\pi^*$ absorption is blue-shifted toward ∼413 nm; likewise, the lower energy MLCT band also undergoes a significant blue-shift toward ∼560 nm. We speculate that such an abrupt shift in absorption could be associated with the spontaneous deprotonation upon depositing TCR dyes on the TiO_2 surface, giving formation of a negatively charged carboxylate that, in turn, could destabilize the π^*-orbital of the bipyridine anchor. In fact, the pK_a of cinchomeronic acid (2.63)[16] was reported to be higher than that of isonicotinic acid (4.9),[17] implying more facile deprotonation for 4,4′,5,5′-tetracarboxy than that for 4,4′-dicarboxy-2,2′-bipyridine. Further evidence of deprotonation is given by the gradual variation of UV/vis absorption spectra by addition of water into the DMF solution (see Figures S4 and S5, Supporting Information). In fact, this experiment would be visualized by the changing of solution color from green to red, which also occurred upon deposition onto TiO_2 and basification mentioned earlier. Moreover, at the DMF/H_2O ratio of 6:4, the recorded spectral patterns are essentially identical to those observed on the TiO_2 thin film, confirming our speculation. In fact, several organic push−pull sensitizers were also reported to exhibit similar blue-shifting of absorption spectra on the TiO_2 surface due to the in situ deprotonation.[18]

We then made a further attempt to deprotonate both sensitizers using tetra-*n*-butyl ammonia hydroxide [TBA]OH (1.0×10^{-2} M) in DMF solution. However, the visual color remained the same even after addition of ≥6 equiv of [TBA]OH. This result is different from the titration experiment using a methanol solution of [TBA]OH at the same concentration, for which a gradual change of color was detected up to an addition of 4−5 equiv of [TBA]OH. Then, an abrupt change to red color was identified after addition of 6 equiv of [TBA]OH. This change of color seems to be not directly proportional to the amount of base added, implying that the proposed deprotonation also critically depends on the protic media (i.e., water or methanol) in the solution. Figure S6 of the Supporting Information depicts the UV−vis absorption spectra of sensitizers at various amounts of added [TBA]OH in methanol.

Cyclic voltammetry was then performed to verify if their HOMOs (the ground-state oxidation potential or $E_{ox}^{\circ\prime}$) matched the redox potential of electrolytic solution for rapid dye regeneration. As shown in Table 1, the onset potentials for oxidation of TCR-1 and TCR-2 on TiO_2 appeared at 0.90 and 0.88 V (vs NHE), respectively, which are attributed to the Ru(II) metal oxidation. These data are more positive than that of the I^-/I_3^- redox couple (ca. 0.4 V vs NHE), confirming the existence of sufficient driving force for the dye regeneration.

Alternatively, the excited-state oxidation potentials ($E^{\circ\prime *}$), e.g., −0.84 and −0.83 V, estimated from the difference of ground-state oxidation potential and the energy gap (E_{0-0}), are more negative than the conduction band potential of the TiO_2 electrode (ca. −0.5 V vs NHE). Furthermore, there are two

dx.doi.org/10.1021/ic501178f | Inorg. Chem. 2014, 53, 8593−8599

Table 1. Electrochemical and Photovoltaic Data of the Studied Ru(II) Sensitizers[a]

dye	$E_{ox}^{\circ\prime}$	E_{0-0}	$E^{\circ\prime}$*	J_{SC}	V_{OC}	FF	η	dye loading
TFRS-2	0.85	1.86	−1.01	16.55	0.64	0.715	7.57	2.05×10^{-7}
TFRS-52	0.83	1.80	−0.97	16.90	0.67	0.716	8.09	1.90×10^{-7}
TCR-1	0.90	1.74	−0.84	13.98	0.61	0.722	6.16	1.08×10^{-7}
TCR-2	0.88	1.71	−0.83	13.73	0.63	0.720	6.23	0.89×10^{-7}

[a] $E_{ox}^{\circ\prime}$ is the redox potential of sensitizer deposited on TiO_2 film. All measurements were in reference to the Fc/Fc^+ standard, and the data were converted to a value relative to NHE (+0.63 V). E_{0-0} was estimated using the onset of the MLCT absorption on the TiO_2 electrode, and $E^{\circ\prime}$* was calculated using the equation $E^{\circ\prime}* = E_{ox}^{\circ\prime} - E_{0-0}$. Open-circuit potential (V_{OC}) of DSC devices is reported in units of V, while short-circuit current density (J_{SC}) and dye loading are in units of $mA \cdot cm^{-2}$ and $mol \cdot cm^{-2}$.

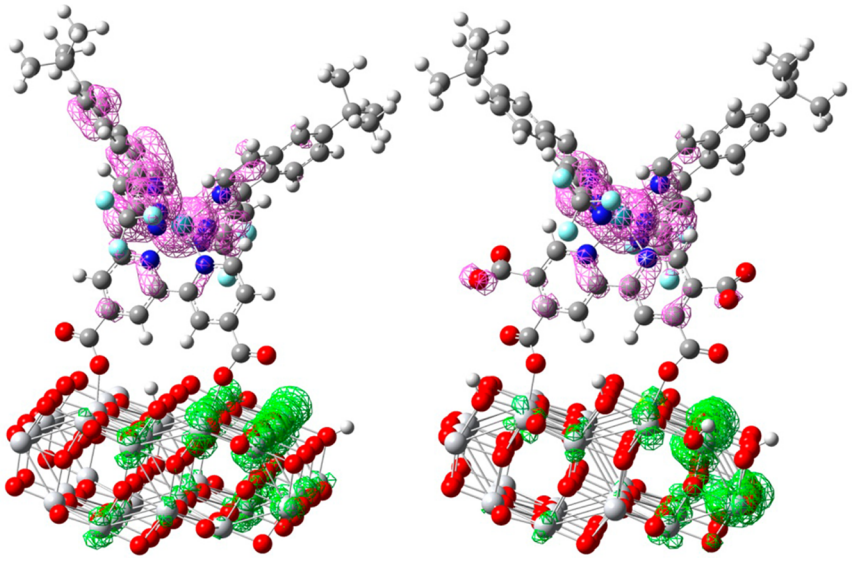

Figure 4. Frontier molecular orbitals HOMO (pink mesh) and LUMO (green mesh) of TFRS-52/$(TiO_2)_{38}$ (left) and TCR-2/$(TiO_2)_{38}$ (right).

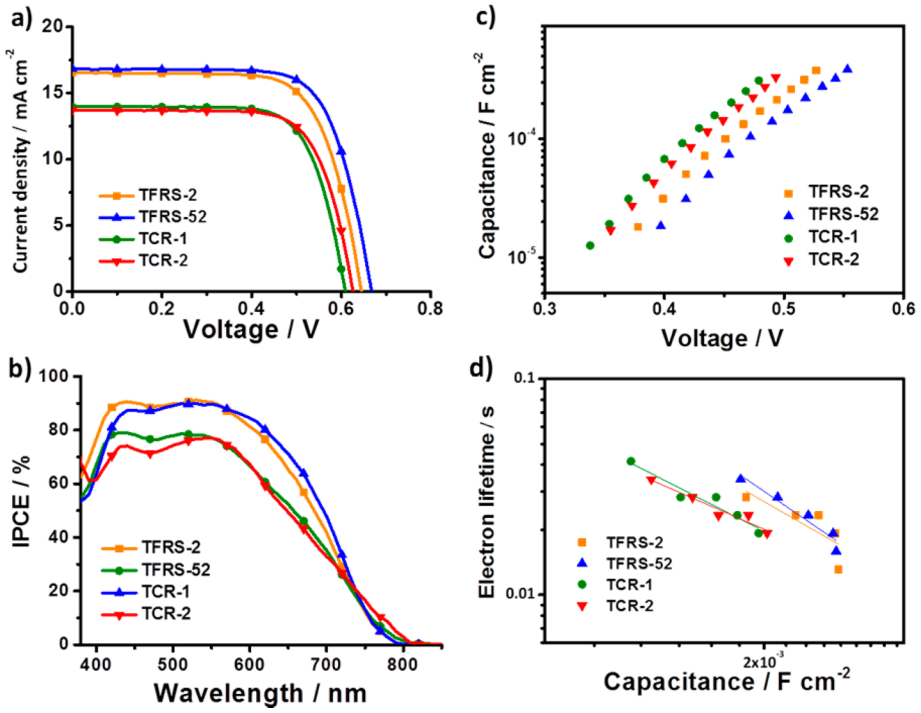

Figure 5. (a) *J*–*V* characteristics. (b) IPCE action diagrams of as-fabricated DSCs. (c) TiO_2 electron density versus voltage deduced from charge extraction measurement. (d) Electron lifetime versus chemical capacitance obtained by IMVS measurement.

viable methods for E_{0-0} measurement, namely, positioning the MLCT shoulder at the 10% maxima,[19] and measuring the interaction between absorption and emission bands.[20] In this study, we use the 10% maxima of the lowest energy absorption

dx.doi.org/10.1021/ic501178f | Inorg. Chem. 2014, 53, 8593−8599

to assess the E_{0-0}, as the UV/vis spectra were measured on samples deposited on TiO_2, while the respective emission on TiO_2 cannot be observed due to the rapid photoinduced electron injection. Moreover, both $E_{ox}^{\circ\prime}$ and $E^{\circ\prime}$* of TCR-1 and TCR-2 are found to be more positive and less negative compared with those of dicarboxy counterparts TFRS-2 and TFRS-52. These observations are consistent with the greater electron deficiency at the Ru(II) metal center and the lowering of the empty π*-orbital energy level of the bipyridine anchor; both are induced by the two extra carboxy groups.

Furthermore, the observed E_{0-0} data are also consistent with those deduced from the simulated TFRS-52/$(TiO_2)_{38}$ and TCR-2/$(TiO_2)_{38}$ models. As shown in Figure 4, the calculated lowest-lying transition involves mainly HOMO → LUMO character, for which HOMO and LUMO are localized at the TFRS-52 (or TCR-2) and the $(TiO_2)_{38}$ surface, respectively, displaying an interfacial electron transfer or the electron injection process from the dye to the $(TiO_2)_{38}$ surface. Similar results are obtained for the optimized TFRS-2/$(TiO_2)_{38}$ and TCR-1/$(TiO_2)_{38}$ models shown in Figure S7 (Supporting Information).

Comparative studies were next executed to reveal their device performances. All DSCs were fabricated using 15 + 7 μm of 20 and 400 nm in diameter of TiO_2 layers and with a projected area of 4 × 4 mm^2 defined by a metal mask. The anodes were stained with 0.3 mM of TCR-1 (or TCR-2) and 0.6 mM deoxycholic acid in a 4:1 volume ratio of mixed ethanol and DMSO solvent over a period of 16 h. The electrolyte consists of 0.6 M PMII, 0.03 M I_2, 0.1 M guanidinium thiocyanate (GuNCS), 0.1 M *t*-BP, and 0.2 M LiI in mixed acetonitrile and valeronitrile (v/v, 85/15). Performances of DSC were then evaluated under 1 sun irradiation (AM 1.5G, 100 mW cm^{-2}), for which the numeric data are summarized in Table 1, while *J*−*V* characteristics and IPCE diagrams are depicted in Figure 5a,b. As can be seen, the efficiency of TCR-1 and TCR-2 was recorded to be 6.16% and 6.23%, respectively. Under identical conditions, the TFRS-2 and TFRS-52 references showed higher efficiencies of 7.57% and 8.09%, respectively. We also like to point out that, upon adoption of an electrolyte with a reduced concentration of LiI, both reference sensitizers have been capable of achieving a DSC efficiency of over 9.5%.[21] In comparison, without this excessive LiI in the electrolyte, DSCs fabricated with TCR-1 and TCR-2 have still afforded a much reduced J_{SC}, showing an insufficient driving force for electron injection. Also, comparing that of TFRS-2 and TFRS-52 references, a slightly lower V_{OC} for TCR-1 and TCR-2 is also noticed (see Figure 5a and Table 1). This can generally be explained by variation of TiO_2 conduction band potential (investigated via charge extraction) and recombination lifetimes (investigated via intensity-modulated photovoltage spectroscopy, IMVS). As showed in Figure 5c, both the TCR-1 and TCR-2 cells feature the higher extracted charge at the same V_{OC} compared with the TFRS-2 and TFRS-52 reference cells, suggesting the downward movement of the TiO_2 conduction band potential.

The inferior DSC performance for TCR-1 and TCR-2, in part, should be due to the fact that the dye loading for both TCR-1 and TCR-2 is significantly less than that of the dicarboxy counterparts TFRS-2 and TFRS-52 (see Table 1). In other words, the above-enhanced deprotonation and the perpendicularly oriented central carboxy groups for TCR-1 (TCR-2) may retard dye absorption, resulting in a smaller dye−TiO_2 association constant (cf. TFRS-2 and TFRS-52). Alternatively, the lower dye loading for the TCR compounds may be consistent with binding through one set of adjacent carboxylate groups at either 4,5- or 4′,5′-positions, which is expected to give a large footprint on the TiO_2 surface. Note that the IMVS measurements at various light intensities (cf. Figure 5d) also showed a decreased electron lifetimes for TCR-1 and TCR-2 cells. Again, this could be attributed to the reduction of dye loading, leading to the increased electron recombination. However, the TiO_2 surface uncovered by sensitizers should effectively interact with the *t*-BP additive in the electrolyte and afford an upward movement of conductive band potentials accordingly.[22] Failure to observe this behavior in the charge extraction experiment suggests the dominance by other factors such as the increased interaction to the dissociated proton, or even Li^+ ions added in the electrolyte.

CONCLUSION

In summary, we have synthesized two Ru(II) sensitizers bearing the 4,4′,5,5′-tetracarboxy-2,2′-bipyridine anchor. Structural data and subsequent spectroscopic studies suggest the increased tendency for deprotonation in solution as well as on the TiO_2 surface. This, together with the simultaneous twisting of the 4,4′-substituted carboxy fragments against the bipyridine chelate, is detrimental to the fabrication of very high efficiency DSC devices. Thus, our works have shown that the excessive introduction of carboxy groups to the sensitizers in the hope of improving cell stability and dye loading may just lead to the opposite consequences, which must be executed with caution.

EXPERIMENTAL SECTION

General Procedures. All purchased commercial chemicals were used without purification. Solvents were dried using a VAC solvent purifier prior to use. All reactions were conducted under an inert N_2 atmosphere. All reactions were monitored by precoated TLC plates (Merck, 0.20 mm with fluorescent indicator UV254). Compounds were visualized using a UVGL-25 Compact UV Lamp. Flash column chromatography was carried out using silica gel with a particle size of 230−400 mesh. Mass spectra were obtained on a JEOL SX-102A instrument operating in electron impact (EI) or fast atom bombardment (FAB) mode. ^{1}H and ^{19}F NMR spectra were measured on a Bruker-400 or INOVA-500 instrument; chemical shifts are quoted with reference to the internal standard Me_4Si. Elemental analysis was carried out with a Heraeus CHN-O Rapid Elementary Analyzer. UV/vis absorption spectra were recorded on a Hitachi U3900 spectrophotometer.

Synthesis of TCR-1-Et. $[RuCl_2(p\text{-cymene})]_2$ (145 mg, 0.23 mmol) and 4,4′,5,5′-tetraethoxycarbonyl-2,2′-bipyridine (200 mg, 0.45 mmol) were added in 30 mL of DMF, and the mixture was heated to 60 °C for 6 h according to literature procedures.[23] After then, DMF was removed under vacuum, and 4-(5-hexylthien-2-yl)-2-(3-(trifluoromethyl)-1*H*-pyrazol-5-yl)pyridine (171 mg, 0.45 mmol), KOAc (221 mg, 2.3 mmol), and xylene (30 mL) were added to the flask. After refluxing for 8 h, the solvent was removed and the crude product was purified by silica gel column chromatography (ethyl acetate:CH_2Cl_2 = 1:10). Yield: 235 mg, 40%. Another Ru(II) derivative, TCR-2-Et, was synthesized from $[RuCl_2(p\text{-cymene})]_2$ and a stoichiometric amount of the respective 6-(*tert*-butyl)-1-(3-(trifluoromethyl)-1*H*-pyrazol-5-yl)isoquinoline using identical procedures.

Selected Spectral Data of TCR-1-Et. ^{1}H NMR (400 MHz, $CDCl_3$, 298 K): δ 8.42 (s, 2H), 8.34 (d, J_{HH} = 3.6 Hz, 2H), 8.31 (s, 2H), 7.73 (d, J_{HH} = 2.0 Hz, 2H), 7.24 (d, J_{HH} = 6.0 Hz, 2H), 7.12 (dd, J_{HH} = 6.0, 2.0 Hz, 2H), 6.99 (s, 2H), 6.79 (d, J_{HH} = 3.6 Hz, 2H), 4.41 (q, J_{HH} = 7.2 Hz, 4H), 4.20 (q, J_{HH} = 7.2 Hz, 4H), 2.82 (t, J_{HH} = 7.2 Hz, 4H), 1.71−1.64 (m, 4H), 1.41−1.27 (m, 18H), 1.15−1.11 (m, 6H), 0.88−0.85 (m, 6H). ^{19}F NMR (376 MHz, $CDCl_3$, 298 K): δ −59.91 (s, 6F).

dx.doi.org/10.1021/ic501178f | Inorg. Chem. 2014, 53, 8593−8599

Selected Spectral Data of TCR-2-Et. ^{1}H NMR (400 MHz, $CDCl_3$, 298 K): δ 8.65 (d, J_{HH} = 9.2 Hz, 2H), 8.30 (s, 2H), 8.24 (s, 2H), 7.76 (dd, J_{HH} = 8.8, 1.6 Hz, 2H), 7.64 (s, 2H), 7.45 (s, 2H), 7.25 (d, J_{HH} = 6.4 Hz, 2H), 7.19 (d, J_{HH} = 6.4 Hz, 2H), 4.39 (q, J_{HH} = 7.2 Hz, 4H), 4.06 (q, J_{HH} = 7.2 Hz, 4H), 1.38 (s, 18H), 1.36−1.34 (m, 6H), 1.26−1.22 (m, 6H). ^{19}F NMR (376 MHz, $CDCl_3$, 298 K): δ −59.89 (s, 6F).

Synthesis of TCR-1. TCR-1-Et (100 mg, 0.08 mmol) was dissolved in a mixed acetone (30 mL) and 2 M $NaOH_{(aq)}$ solution (2 mL). After stirring for 8 h, the solvent was evaporated under vacuum and the residue was dissolved in 10 mL of H_2O and titrated with 2 N HCl to pH 3 to induce a black precipitation. This black product was washed with a small amount of deionized water and acetone in sequence, to yield TCR-1 (69 mg, 76%). Another Ru(II) derivative, TCR-2, was synthesized by hydrolysis of the obtained TCR-2-Et using identical procedures.

Selected Spectral Data of TCR-1. MS (FAB, ^{102}Ru): m/z 1189.1 $(M + 1)^+$. ^{1}H NMR (400 MHz, d_6-DMSO, 298 K): δ 9.07 (s, 2H), 8.38 (s, 2H), 8.31 (s, 2H), 7.77 (d, J_{HH} = 2.8 Hz, 2H), 7.56 (s, 2H), 7.48 (d, J_{HH} = 5.6 Hz, 2H), 7.13 (d, J_{HH} = 6.0 Hz, 2H), 6.97 (d, J_{HH} = 2.8 Hz, 2H), 2.82 (t, J_{HH} = 7.2 Hz, 4H), 1.64−1.62 (m, 4H), 1.31−1.26 (m, 12H), 0.85−0.83 (m, 6H). ^{19}F NMR (376 MHz, d_6-DMSO, 298 K): δ −58.16 (s, 6F). Anal. Calcd for $C_{52}H_{46}F_6N_8O_8RuS_2\cdot 2H_2O$: C, 50.93; N, 9.14; H, 4.11. Found: C, 50.65; N, 9.16; H, 4.09.

Selected Spectral Data of TCR-2. MS (FAB, ^{102}Ru): m/z 1069.9 $(M + 1)^+$. ^{1}H NMR (400 MHz, d_6-DMSO, 298 K): δ 8.97 (s, 2H), 8.79 (d, J_{HH} = 8.8 Hz, 2H), 8.72 (s, 2H), 7.87 (d, J_{HH} = 9.2 Hz, 2H), 7.83 (s, 2H), 7.77 (s, 2H), 7.56 (d, J_{HH} = 6.8 Hz, 2H), 7.05 (d, J_{HH} = 6.4 Hz, 2H), 1.36 (s, 18H). ^{19}F NMR (376 MHz, d_6-DMSO, 298 K): δ −57.93 (s, 6F). Anal. Calcd for $C_{48}H_{38}F_6N_8O_4Ru\cdot 3H_2O$: C, 51.29; N, 9.97; H, 3.95. Found: C, 51.49; N, 9.82; H, 4.12.

Device Fabrication. TCR-1 and TCR-2 sensitizers were selected for fabrication of the DSCs using a standard method, for which the mesoporous TiO_2 photoanode was screen-printed on an FTO glass using a 15 μm adsorbing layer (20 nm) and a 7 μm light-scattering layer (400 nm). For preparation of the dye solution, the sensitizer (0.3 mM) was dissolved in a mixture of EtOH and DMSO (v/v, 4/1), along with the addition of 0.6 mM DCA as coadsorbate for suppressing aggregation. The electrolyte consists of 0.6 M PMII, 0.03 M I_2, 0.1 M guanidinium thiocyanate (GuNCS), 0.1 M *t*-BP, and 0.2 M LiI in a mixture of acetonitrile and valeronitrile (v/v, 85/15). The dye loading is estimated from the relative ratio of the MLCT absorption band of the desorbed dye versus the reference solution in 0.01 mM; both are in mixed MeOH and water (v/v, 1:1) with addition of 0.1 M TBAOH. The solar cells were covered with a black metal mask with an aperture (0.4 × 0.4 cm^2) to define the active area during measurement.

X-ray Crystallography. All single-crystal X-ray diffraction data were measured on a Bruker Smart CCD diffractometer using λ (Mo Kα) radiation (λ = 0.71073 Å). The data collection was executed using the SMART program. Cell refinement and data reduction were made with the SAINT program. The structure was determined using the SHELXTL/PC program and refined using full-matrix least-squares.[24] All non-hydrogen atoms were refined anisotropically, whereas hydrogen atoms were placed at the calculated positions and included in the final stage of refinements with fixed parameters. However, serious disorders were observed for both the CF_3 substituents and the hexyl appendages of the pyridyl pyrazolate ancillaries, due to the loose packing of molecules within the crystal lattices.

■ ASSOCIATED CONTENT

Ⓢ Supporting Information

X-ray structural data of ester derivative TCR-1-Et in CIF format. Synthetic procedures for 4,4′,5,5′-tetraethoxycarbonyl-2,2′-bipyridine, experimental details for TDDFT and DFT computation, electrochemistry and photovoltaic characterization, and computational results and UV/vis spectral analyses of both TCR-1 and TCR-2. This material is available free of charge via the Internet at http://pubs.acs.org.

■ AUTHOR INFORMATION

Corresponding Authors

*E-mail: ychi@mx.nthu.edu.tw (Y.C.).

*E-mail: chop@ntu.edu.tw (P.-T.C.).

Notes

The authors declare no competing financial interest.

■ ACKNOWLEDGMENTS

This work was supported by the Ministry of Science and Technology, Taiwan, and the computation was executed using the facility at the National Center for High-Performance Computing (NCHC).

■ REFERENCES

(1) (a) Hagfeldt, A.; Boschloo, G.; Sun, L.; Kloo, L.; Pettersson, H. *Chem. Rev.* **2010**, *110*, 6595. (b) Bai, Y.; Mora-Seró, I.; De Angelis, F.; Bisquert, J.; Wang, P. *Chem. Rev.* **2014**, DOI: 10.1021/cr400606n.

(2) Cheng, Y.-J.; Yang, S.-H.; Hsu, C.-S. *Chem. Rev.* **2009**, *109*, 5868.

(3) (a) Heo, J. H.; Im, S. H.; Noh, J. H.; Mandal, T. N.; Lim, C.-S.; Chang, J. A.; Lee, Y. H.; Kim, H.-J.; Sarkar, A.; Nazeeruddin, M. K.; Gratzel, M.; Seok, S. I. *Nat. Photonics* **2013**, *7*, 486. (b) Eperon, G. E.; Stranks, S. D.; Menelaou, C.; Johnston, M. B.; Herz, L. M.; Snaith, H. J. *Energy Environ. Sci.* **2014**, *7*, 982.

(4) (a) Nazeeruddin, M. K.; Péchy, P.; Renouard, T.; Zakeeruddin, S. M.; Humphry-Baker, R.; Comte, P.; Liska, P.; Cevey, L.; Costa, E.; Shklover, V.; Spiccia, L.; Deacon, G. B.; Bignozzi, C. A.; Grätzel, M. *J. Am. Chem. Soc.* **2001**, *123*, 1613. (b) Chiba, Y.; Islam, A.; Watanabe, Y.; Komiya, R.; Koide, N.; Han, L. *Jpn. J. Appl. Phys.* **2006**, *45*, L638. (c) Chen, B.-S.; Chen, K.; Hong, Y.-H.; Liu, W.-H.; Li, T.-H.; Lai, C.-H.; Chou, P.-T.; Chi, Y.; Lee, G.-H. *Chem. Commun.* **2009**, 5844.

(5) (a) Yen, Y.-S.; Chou, H.-H.; Chen, Y.-C.; Hsu, C.-Y.; Lin, J. T. *J. Mater. Chem.* **2012**, *22*, 8734. (b) Zhang, M.; Wang, Y.; Xu, M.; Ma, W.; Li, R.; Wang, P. *Energy Environ. Sci.* **2013**, *6*, 2944. (c) Liang, M.; Chen, J. *Chem. Soc. Rev.* **2013**, *42*, 3453.

(6) Qin, C.; Wong, W.-Y.; Han, L. *Chem.—Asian J.* **2013**, *8*, 1706.

(7) Mathew, S.; Yella, A.; Gao, P.; Humphry-Baker, R.; CurchodBasile, F. E.; Ashari-Astani, N.; Tavernelli, I.; Rothlisberger, U.; Nazeeruddin, M. K.; Grätzel, M. *Nat. Chem.* **2014**, *6*, 242.

(8) (a) Chang, S.; Wang, H.; Hua, Y.; Li, Q.; Xiao, X.; Wong, W.-K.; Wong, W. Y.; Zhu, X.; Chen, T. *J. Mater. Chem. A* **2013**, *1*, 11553. (b) Hua, Y.; Chang, S.; Huang, D.; Zhou, X.; Zhu, X.; Zhao, J.; Chen, T.; Wong, W.-Y.; Wong, W.-K. *Chem. Mater.* **2013**, *25*, 2146. (c) Hua, Y.; Chang, S.; He, J.; Zhang, C.; Zhao, J.; Chen, T.; Wong, W.-Y.; Wong, W.-K.; Zhu, X. *Chem.—Eur. J.* **2014**, *20*, 6300.

(9) (a) Chen, K.; Hong, Y.-H.; Chi, Y.; Liu, W.-H.; Chen, B.-S.; Chou, P.-T. *J. Mater. Chem.* **2009**, *19*, 5329. (b) Hewat, T.; McDonald, S.; Lee, J.; Rahman, M.; Cameron, P.; Hu, F.-C.; Chi, Y.; Yellowlees, L. J.; Robertson, N. *RSC Adv.* **2014**, *4*, 10165.

(10) (a) Yang, S.-H.; Wu, K.-L.; Chi, Y.; Cheng, Y.-M.; Chou, P.-T. *Angew. Chem., Int. Ed.* **2011**, *50*, 8270. (b) Funaki, T.; Funakoshi, H.; Kitao, O.; Onozawa-Komatsuzaki, N.; Kasuga, K.; Sayama, K.; Sugihara, H. *Angew. Chem., Int. Ed.* **2012**, *51*, 7528. (c) Wu, K.-L.; Li, C.-H.; Chi, Y.; Clifford, J. N.; Cabau, L.; Palomares, E.; Cheng, Y.-M.; Pan, H.-A.; Chou, P.-T. *J. Am. Chem. Soc.* **2012**, *134*, 7488. (d) Numata, Y.; Singh, S. P.; Islam, A.; Iwamura, M.; Imai, A.; Nozaki, K.; Han, L. *Adv. Funct. Mater.* **2013**, *23*, 1817. (e) Chou, C.-C.; Hu, F.-C.; Yeh, H.-H.; Wu, H.-P.; Chi, Y.; Clifford, J. N.; Palomares, E.; Liu, S.-H.; Chou, P.-T.; Lee, G.-H. *Angew. Chem., Int. Ed.* **2014**, *53*, 178.

(11) (a) Argazzi, R.; Bignozzi, C. A.; Heimer, T. A.; Castellano, F. N.; Meyer, G. J. *Inorg. Chem.* **1994**, *33*, 5741−5749. (b) Dai, F.-R.; Wu, W.-J.; Wang, Q.-W.; Tian, H.; Wong, W.-Y. *Dalton Trans.* **2011**, *40*, 2314.

(12) Geary, E. A. M.; Yellowlees, L. J.; Jack, L. A.; Oswald, I. D. H.; Parsons, S.; Hirata, N.; Durrant, J. R.; Robertson, N. *Inorg. Chem.* **2004**, *44*, 242.

(13) (a) Zong, R.; Wang, D.; Hammitt, R.; Thummel, R. P. *J. Org. Chem.* **2005**, *71*, 167−175. (b) Haberecht, M. C.; Schnorr, J. M.;

Andreitchenko, E. V.; Clark, C. G.; Wagner, M.; Müllen, K. *Angew. Chem., Int. Ed.* **2008**, *47*, 1662.
(14) Ozawa, H.; Oura, S.; Shimizu, R.; Arakawa, H. *Chem. Lett.* **2012**, *41*, 1406.
(15) (a) De Angelis, F.; Tilocca, A.; Selloni, A. *J. Am. Chem. Soc.* **2004**, *126*, 15024. (b) Liu, S.-H.; Fu, H.; Cheng, Y.-M.; Wu, K.-L.; Ho, S.-T.; Chi, Y.; Chou, P.-T. *J. Phys. Chem. C* **2012**, *116*, 16338.
(16) Perrin, D. D. *Dissociation Constants of Organic Bases in Aqueous Solution: Supplement*; Butterworths: London, 1972.
(17) Serjeant, E. P.; Dempsey, B. *Ionization Constants of Organic Acids in Aqueous Solution*; Pergamon: Oxford, U.K., 1979.
(18) (a) Yella, A.; Humphry-Baker, R.; Curchod, B. F. E.; Ashari Astani, N.; Teuscher, J.; Polander, L. E.; Mathew, S.; Moser, J.-E.; Tavernelli, I.; Rothlisberger, U.; Grätzel, M.; Nazeeruddin, M. K.; Frey, J. *Chem. Mater.* **2013**, *25*, 2733. (b) Wu, Y.; Zhu, W. *Chem. Soc. Rev.* **2013**, *42*, 2039.
(19) Numata, Y.; Islam, A.; Sodeyama, K.; Chen, Z.-H.; Tateyama, Y.; Han, L. *J. Mater. Chem. A* **2013**, *1*, 11033.
(20) El-Shafei, A.; Hussain, M.; Islam, A.; Han, L. *J. Mater. Chem. A* **2013**, *1*, 13679.
(21) (a) Wu, K.-L.; Hsu, H.-C.; Chen, K.; Chi, Y.; Chung, M.-W.; Liu, W.-H.; Chou, P.-T. *Chem. Commun.* **2010**, *46*, 5124. (b) Wang, S.-W.; Wu, K.-L.; Ghadiri, E.; Lobello, M. G.; Ho, S.-T.; Chi, Y.; Moser, J.-E.; De Angelis, F.; Grätzel, M.; Nazeeruddin, M. K. *Chem. Sci.* **2013**, *4*, 2423. (c) Wu, K.-L.; Ku, W.-P.; Clifford, J. N.; Palomares, E.; Ho, S.-T.; Chi, Y.; Liu, S.-H.; Chou, P.-T.; Nazeeruddin, M. K.; Grätzel, M. *Energy Environ. Sci.* **2013**, *6*, 859.
(22) (a) Haque, S. A.; Palomares, E.; Cho, B. M.; Green, A. N. M.; Hirata, N.; Klug, D. R.; Durrant, J. R. *J. Am. Chem. Soc.* **2005**, *127*, 3456. (b) Nakade, S.; Kanzaki, T.; Kubo, W.; Kitamura, T.; Wada, Y.; Yanagida, S. *J. Phys. Chem. B* **2005**, *109*, 3480.
(23) Hu, F.-C.; Wang, S.-W.; Chi, Y.; Robertson, N.; Hewat, T.; Hu, Y.; Liu, S.-H.; Chou, P.-T.; Yang, P.-F.; Lin, H.-W. *ChemPhysChem* **2014**, *15*, 1207.
(24) Sheldrick, G. M. *Acta Crystallogr., Sect. A: Found. Crystallogr.* **2008**, *64*, 112.